



Research paper

Monitoring and control of steel truss arch bridge jacking construction

Xilong Zheng¹, Di Guan²

Abstract: Through the real-time monitoring of the internal force, alignment and suspender force in the process of bridge jacking construction, the measured data and theoretical calculation values obtained from the monitoring are compared and analyzed, and it is found that the measured data are in good agreement with the theoretical calculation values. The results show that through the analysis of the real-time monitoring data of the jacking process of the bridge, the measured stress values of the main beam are within the range of -40.79 MPa \sim 25.13 MPa, and the measured stress of the main arch is within -40.33 MPa \sim 16.06 MPa, which does not exceed the allowable stress range of the steel in the jacking process, and the structure is safe. The measured elevation of the line is in good agreement with the theoretical elevation, and the deviation is mostly less than 5 mm, and the maximum deviation does not exceed the limit value of 8mm. The difference between the measured cable force and the designed cable force in the stage of removing the temporary pier is very small, which does not exceed $\pm 5\%$ and meets the requirements of the specification. The research in this paper can provide a reference for the jacking construction of similar bridges.

Keywords: steel truss arch bridge, incremental launching construction, construction monitoring

¹PhD., Harbin University, School of Civil and Architectural Engineering, No.109 Zhongxing Da Dao, Harbin, China, e-mail: sampson88@126.com, ORCID: [0000-0001-5571-667X](https://orcid.org/0000-0001-5571-667X)

²M.Sc., Harbin University, School of Civil and Architectural Engineering, No.109 Zhongxing Da Dao, Harbin, China, e-mail: 996349518@qq.com, ORCID: [0009-0006-2965-806X](https://orcid.org/0009-0006-2965-806X)

1. Introduction

With the development of society and the advancement of technology, there are now increasingly diverse styles of bridge structures, with larger spans. Among the various types of bridges, steel truss arch bridges not only have high stiffness but also possess a visually appealing appearance. Before the 1980s, aesthetically pleasing, plasticity and toughness, and high load-carrying capacity steel truss arch bridges were widely utilized [1–5].

The selection of the most suitable construction method for bridge construction is usually based on factors such as local topography, the purpose of the bridge, and construction costs. In recent years, the top-down construction method has been widely applied in bridge construction, mostly in cases where the terrain is complex, there is a need for water passage underneath the bridge, and it is not feasible to set up supports beneath the bridge [6–8]. For steel truss arch bridges, due to their beautiful appearance, lightweight form, and ability to blend well with the surrounding environment, they have been widely employed in urban landscape bridges [9–11]. Research on the top-down construction method in China has mostly focused on prestressed concrete beams and has achieved fruitful results. However, due to certain characteristics of steel box girders, such as no prestressing, high rigidity, and local stability, the research findings on top-down construction of prestressed concrete beams cannot be directly applied to steel box girders. Therefore, it is particularly important to conduct research on top-down construction of steel box girder structures [12–14].

During the entire top-down process of a steel truss arch bridge, the main structure undergoes multiple steps such as lifting, dragging, system conversion, and alignment. The main structure needs to possess good strength and stiffness to ensure the smooth and safe progress of the top-down construction process. Real-time monitoring is required during the construction process to ensure its success. Existing research has mostly concentrated on construction monitoring of concrete bridges, and there is insufficient data available for reference in the construction monitoring of steel truss arch bridges [15–18]. In most studies on top-down construction of steel arch bridge structures, the traditional approach is to separate the beam and the arch during top-down construction, meaning that the main girder is first pushed, followed by the pushing of the arch ribs. Examples of employing the holistic top-down approach are relatively rare. In this study, based on real-time monitoring results during the top-down construction process of the supporting project, the measured data obtained from monitoring is compared and analyzed against theoretical calculations to determine if the internal forces of the structure are within a safe state.

2. Engineering background introduction

This paper is based on a steel truss arch bridge project. The main bridge structure adopts a downward steel truss arch beam structure with a main span of 106 m and a full width of 38 m, including a 24 m-wide roadway with six lanes in both directions. The main beam is a structure that is jointly supported by main longitudinal beams, steel cross beams, and secondary longitudinal beams. The bridge deck consists of orthogonal-shaped plates, and the beam height at the centerline of the bridge is 2.565 m. The steel used is of type Q345qC. The

main arch ribs of the bridge are in the form of steel truss. There are upper and lower layers of arch ribs connected by vertical and diagonal bracing to form a unified structure. Two girders are placed horizontally and connected by transverse struts to enhance lateral stability. The span of the upper arch rib is approximately 142 m with a rise of 23.5 m, while the span of the lower arch rib is approximately 103 m with a rise of 20 m. The net rise of the truss arch is 19.288 m, and the rise-to-span ratio is 1:5.5. There is a 3.5 m difference in height between the top of the upper arch rib and the top of the lower arch rib. Parallel steel cable suspenders are used for this bridge, and a total of 30 suspenders are arranged. The lower end of each suspender is anchored to the corresponding ear plate of the main longitudinal beam cross beam, while the upper end is anchored to the corresponding ear plate on the transverse partition plate inside the arch rib box. Reinforcing ribs are set on both sides of the ear plate, serving as the main force transmission components. The weight of the bridge's truss steel structure is 3816 t, the weight of the suspenders is 10.7 t, the weight of the assembled arch ring support is 123.1 t, and the weight of the guide beam is 83.8 t with a length of 25 m. The construction of the project adopts the top-down method with continuous multi-point pushing. The construction diagram of the pushing process is shown in Fig. 1. The elevation layout and cross-section layout of the bridge are shown in Fig. 2 to Fig. 3.



Fig. 1. The construction drawing for top-down construction of a steel truss arch bridge

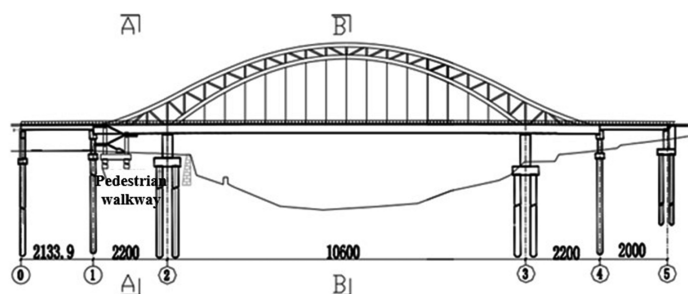


Fig. 2. Bridge elevation layout drawing (unite:cm)

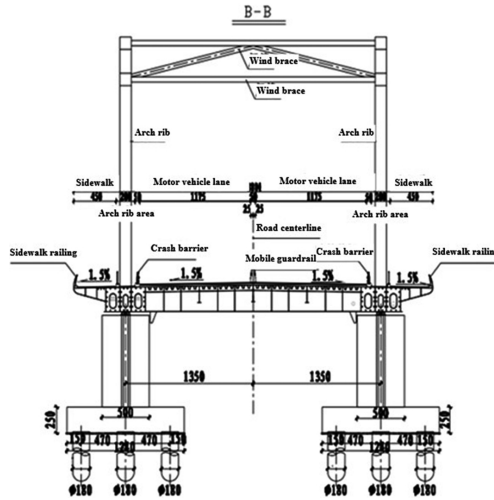


Fig. 3. Cross-section layout drawing (unite:cm)

3. Introduction to the integral top-down construction process

Due to the navigational requirements of the river flowing under the bridge, it is not possible to construct scaffolding in the river. Therefore, the main bridge steel truss arch bridge is constructed using the integral top-down method. The main construction steps are as follows, as shown in Table 1 to Table 8. Adaptive control method is adopted in bridge construction monitoring. Ensure that the internal force and deformation of the bridge structure are always within the allowable safety range during construction, and ensure that the state of the bridge meets the design requirements.

Table 1. Top-down construction process step one

Step one	Construction preparation
Construction schematic	<p>The schematic shows a sequence of 16 numbered steps. Steps 1 through 5 are on the left side, steps 6 through 10 are in the middle, and steps 11 through 16 are on the right side. The steps illustrate the installation of temporary support piers and the arrangement of jacks and beams.</p>
Content description	<p>Set up two temporary support piers, L1 and L2, between piers 2 and 3. Install sliding beam tracks on the temporary support piers and arrange the installation of horizontal and vertical jacks for adjustment purposes. Conduct testing and adjustment of the top pushing equipment.</p>

Table 2. Top-down construction process step two

Step two	Assembly of beam arch structure
Construction schematic	
Content description	<p>Assemble the steel box girder structure, arch ribs, suspension rods, and guide beams at the assembly site. After installing the suspension rods, apply a certain amount of prestressing force as required. Install the pier top pushing and alignment systems and adjust them accordingly. Once the top pushing system is ready, perform the necessary tests and adjustments.</p>

Table 3. Top-down construction process step three

Step three	The jacking operation is in progress
Construction schematic	
Content description	<ol style="list-style-type: none"> 1. Start the pulling device and drag the steel beam forward by 33.75 m. 2. Activate the vertical jacks to detach the steel beam from the sliders. Move all the sliders back to the starting position of the pulling device. 3. The rear cantilever is 26.96 m long.

Table 4. Top-down construction process step four

Step four	The jacking operation is in progress
Construction schematic	
Content description	<ol style="list-style-type: none"> 1. Start the pulling device and drag the steel beam forward for 33 m. 2. Activate the vertical jack to separate the steel beam from the sliders; move all the sliders back to the initial position of the pulling device. 3. The tail overhangs for 26.96 m.

Table 5. Top-down construction process step five

Step five	The jacking operation is in progress
Construction schematic	
Content description	<ol style="list-style-type: none"> 1. Start the pulling device and drag the steel beam forward for 33.75 m. 2. During the dragging process, dismantle the steel guide beams section by section. 3. Activate the vertical jack to separate the steel beam from the sliders; move all the sliders back to the initial position of the pulling device. 4. The tail overhangs for 26.96 m.

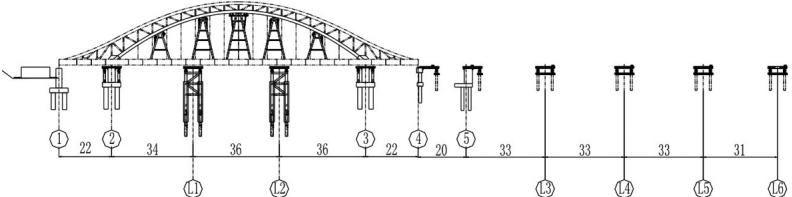
Table 6. Top-down construction process step six

Step six	The jacking operation is in progress
Construction schematic	
Content description	<ol style="list-style-type: none"> 1. Start the pulling device and drag the steel beam forward for 33 m. 2. During the dragging process, dismantle the steel guide beams section by section. 3. Activate the vertical jack to separate the steel beam from the sliders; move all the sliders back to the initial position of the pulling device. 4. The tail overhangs for 10.5 m.

Table 7. Top-down construction process step seven

Step seven	The jacking operation is in progress
Construction schematic	
Content description	<ol style="list-style-type: none"> 1. Start the pulling device and drag the steel beam forward for 17.25 m. 2. Drag the steel beam into its final position.

Table 8. Top-down construction process step eight

Step eight	The jacking operation is in progress
Construction schematic	
Content description	<ol style="list-style-type: none"> 1. Activate the vertical jack to separate the steel beam from the sliders and use the three jacks to adjust the final position of the steel beam. 2. Dismantle the dragging sliders layer by layer to complete the overall placement of the beam.

4. Construction monitoring plan

The model consists of 1389 nodes and 1728 elements of various types. The finite element model can be seen in Fig. 4. The main beam and arch ribs are made of beam elements, and the suspender is made of truss elements. According to the construction process, the analysis is divided into 34 construction stages, with each stage advancing the structure by 5 m. The main construction stages include the steel truss beam jacking stage and the maximum cantilever stage. Each construction stage activates the corresponding structural groups or boundary groups based on the actual conditions. The analysis simulates the stress and deformation of the main structure in each construction stage.

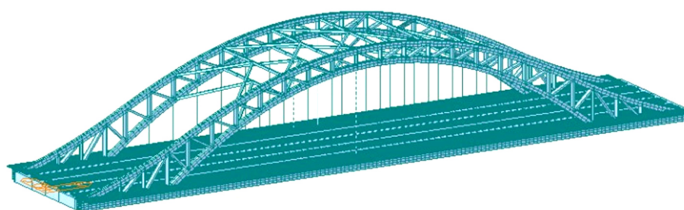


Fig. 4. Calculation model of a steel truss arch bridge

5. Construction monitoring plan

5.1. Stress monitoring measurement points

Strain measurement point arrangement sectional diagram is shown in Fig. 5. There are five monitoring sections on the main beam, namely D1–D5 sections. The schematic diagram of strain measurement point arrangement on the main beam is shown in Fig. 6, with 4 strain measurement points arranged on each transverse section. Four sensors are placed at the

maximum cantilever section in front of the main beam at D1 section, and four sensors are placed at the maximum cantilever section at the rear at D5 section. Four sensors are placed at the mid-span section at D3 position, and four sensors are respectively placed at L/4 section at D2 and D4 positions. The strain gauges are connected to the bridge deck, and strain data is collected using a strain acquisition device to monitor the stress during the entire steel box girder top-down pushing process. The elevation is measured every 10 mins, and the distance of the bridge is not more than 20 cm.

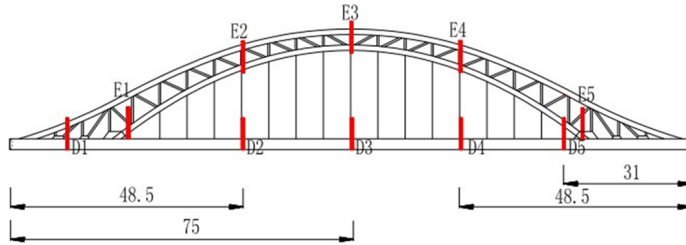


Fig. 5. Strain gauge placement cross-section schematic

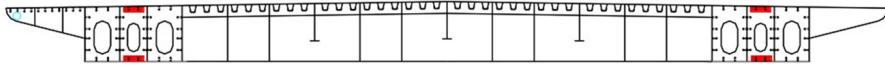


Fig. 6. Cross-sectional schematic diagram of strain gauge placement on the main beam

The main beam stress measurement sensors use steel-wire surface strain gauges, as shown in Fig. 7.



Fig. 7. Surface strain gauge placement diagram on the main beam

The schematic diagram of the arch rib strain measurement point arrangement is shown in Fig. 8, with two strain measurement points arranged on each transverse section. The most critical sections of the arch rib are the arch crown section, the L/4 section (L is the span), and the two side foot sections. On each section, a steel cord surface strain gauge is placed on the top and bottom surfaces of the arch rib to measure the stress-strain behavior of the steel arch rib, as shown in Fig. 9.

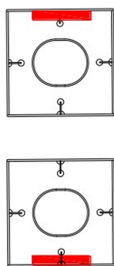


Fig. 8. Schematic diagram of strain gauge placement on the arch rib



Fig. 9. Surface strain gauges on the arch rib

5.2. Setting of pre-arched curvature

Pre-arch curvature, also known as pre-camber value, is set to counteract the deflection generated by the main beam, main arch, and other structures under load, with the aim of controlling the linearity of the structure. During construction, a pre-determined value is set in the opposite direction of the downward deflection of the main structure. In actual projects, the deflection of the structure is usually strictly controlled to achieve the desired design profile. However, simply limiting the deflection may not effectively improve the stiffness of the structure. Therefore, when designing the profile of the main beam, if the main beam can be designed with an upwardly arched curve of a certain radius in advance, the profile and stiffness of the main beam will achieve the desired design effect. For simply supported beam bridges, the pre-arch curvature value at mid-span should be chosen as the deflection value generated when both sustained load and live load are applied simultaneously, in the opposite direction.

Equation (5.1) is as follows:

$$(5.1) \quad f = f_q + \frac{1}{2}f_p$$

where: f – mid-span pre-arch curvature value, f_q – mid-span deflection value caused by sustained load, f_p – Mid-span deflection value caused by live load.

5.3. Main beam deformation

The selection of control points for main beam alignment includes eight longitudinal bridge cross-sections. Based on the actual construction and design characteristics of the bridge, the main focus is on controlling the deflection variation of the bridge, which is symmetrical on both sides. Therefore, three measurement points are selected for each main beam cross-section, specifically on both sides of the main beam and at the mid-span. For ease of documentation, the measurement points are labeled as A1, A2, A3, A4, B1, C1, C2, C3. The point with the maximum deflection, selected based on the variation of the top pushing distance, is chosen as the control point for alignment. The arrangement of measurement points is shown in Fig. 10 to Fig. 11. The elevation is measured every 10 mins, and the distance of the bridge is not more than 20 cm.

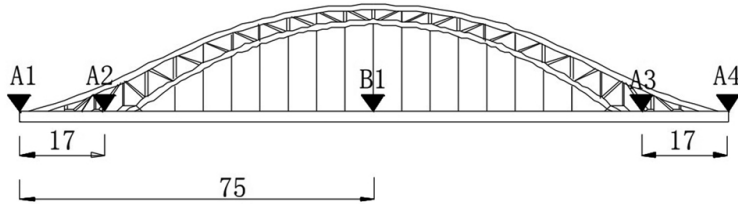


Fig. 10. Elevation measurement points on the main beam during the jacking process

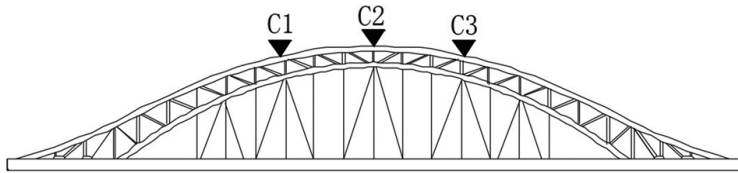


Fig. 11. Elevation measurement points on the arch crown during the jacking process

5.4. Suspension rod tension monitoring

Suspension rod tension testing is commonly done using the vibration method, which is currently the most widely used approach. The principle of this method involves attaching a vibration exciter at appropriate positions on the suspension rod. By striking the rod, vibrations are induced, and the frequency of these vibrations is analyzed using a tension measuring instrument to determine the tension value.

During construction, various factors such as construction errors, structural self-weight, and stiffness can result in deviations between the actual state of the suspension rod and the theoretical state. Therefore, to achieve the desired tension values for the suspension rods, adjustments should be made after the completion of the main beam support and when the bridge is in its final state. This ensures that the tension values are in the ideal range.

In the case of your particular bridge, there are a total of 30 suspension rods, and the layout of the tension control points for these rods is shown in Fig. 12.

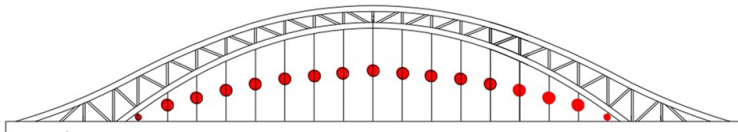


Fig. 12. Schematic diagram of the layout of force control points for suspension rods

6. Analysis of construction monitoring results

6.1. Stress monitoring results

The measured stress values during various construction stages show a consistent trend with the theoretical stress values, indicating that the spatial model established through finite element software can effectively simulate the jacking construction process. This method demonstrates a certain level of rationality.

The comparison of stress distribution from D1 cross section to D5 cross section are shown in Fig. 13 to Fig. 17. During the jacking process, the measured stress values of the main beam range from -40.79 MPa to 25.13 MPa, which fall within the allowable stress range. The structural safety during the jacking process is ensured. Observation reveals that the D5 section exhibits larger stress fluctuations compared to other sections. This is because the D5 section is the most unfavorable section at the tail end of the main beam. Without the installation of a back-span, the stress at this section reaches its peak whenever the tail end is in the maximum cantilever state.

The method of multi-point continuous jacking through dragging relies on the support of temporary and permanent piers along the jacking route to push the main structure forward. During the jacking process, the maximum stress values occur at each section when it passes through the temporary jacking piers.

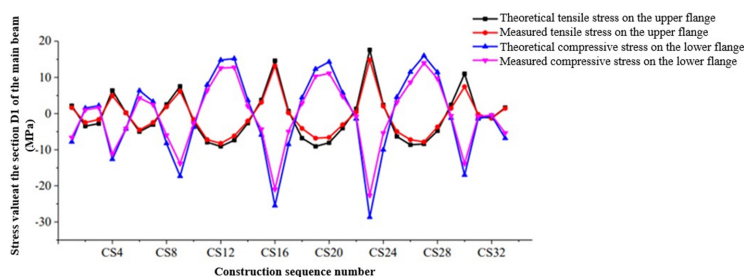


Fig. 13. Comparison diagram of stress distribution on cross-section D1

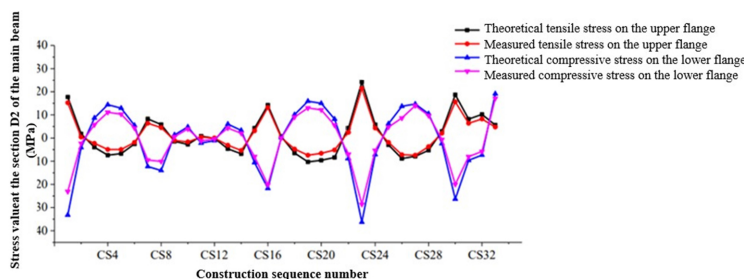


Fig. 14. Comparison diagram of stress distribution on cross-section D2

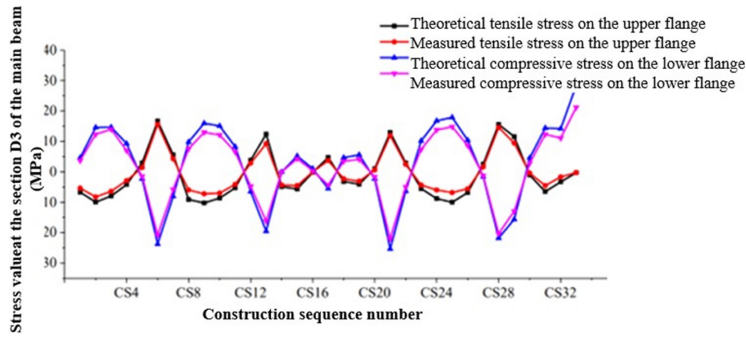


Fig. 15. Comparison diagram of stress distribution on cross-section D3

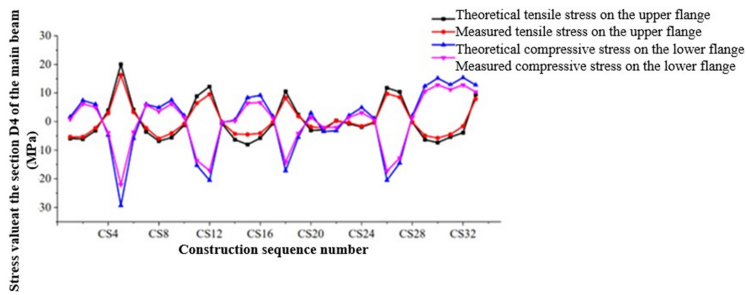


Fig. 16. Comparison diagram of stress distribution on cross-section D4

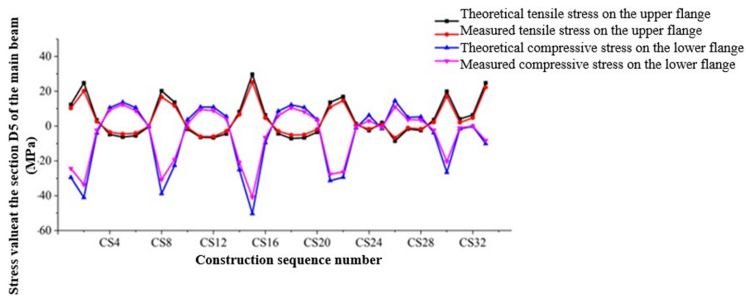


Fig. 17. Comparison diagram of stress distribution on cross-section D5

The measured stress values during each major construction stage show a consistent trend with the theoretical stress values, further confirming the accuracy and effectiveness of the finite element spatial model simulation.

The stress comparison between E1 section and E5 section of arch rib are shown in Fig. 18 to Fig. 22. During the jacking process, the stress values of the main arch range from -40.33 MPa to 16.06 MPa, indicating a relatively stable load distribution. The stress values remain within the allowable stress range of the steel material during the jacking process, ensuring the structural safety. Throughout the jacking process, the main arch and main beam exhibit similar stress characteristics, with the maximum stress values occurring at each section when it passes through the temporary jacking piers.

After the removal of the temporary piers, significant changes in stress are observed in the main arch. This is mainly due to the different boundary conditions of the main beam before and after the removal of the temporary piers, which is a normal phenomenon.

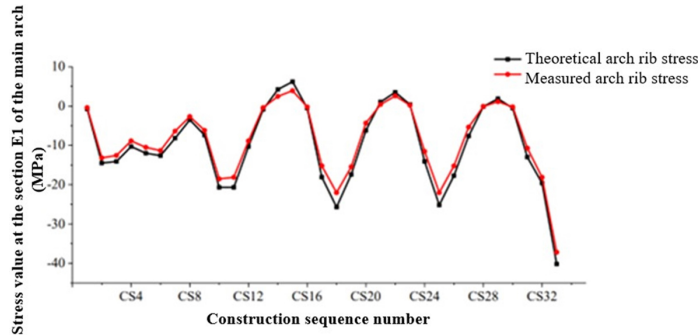


Fig. 18. Comparison values of stress on arch ribs on section E1

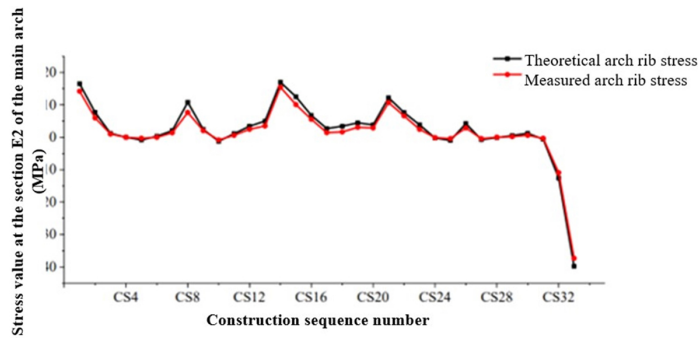


Fig. 19. Comparison values of stress on arch ribs on section E2

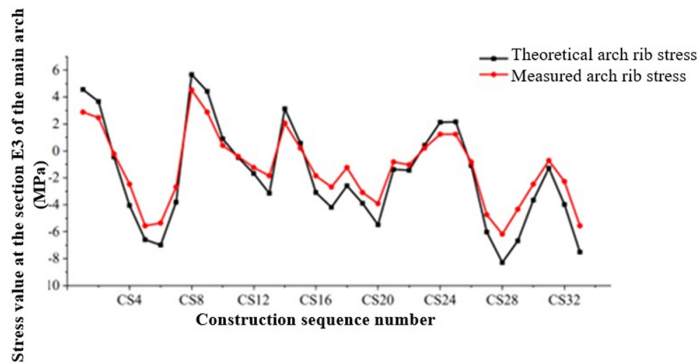


Fig. 20. Comparison values of stress on arch ribs on section E3

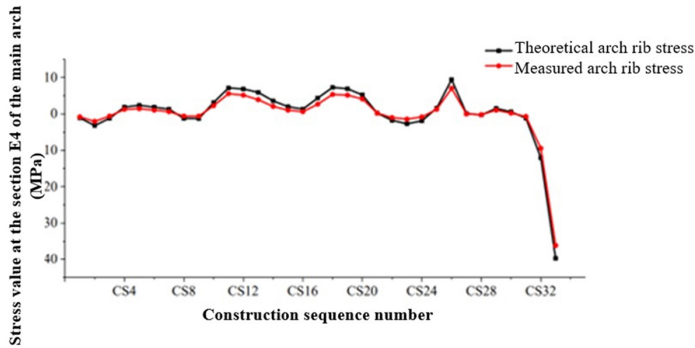


Fig. 21. Comparison values of stress on arch ribs on section E4

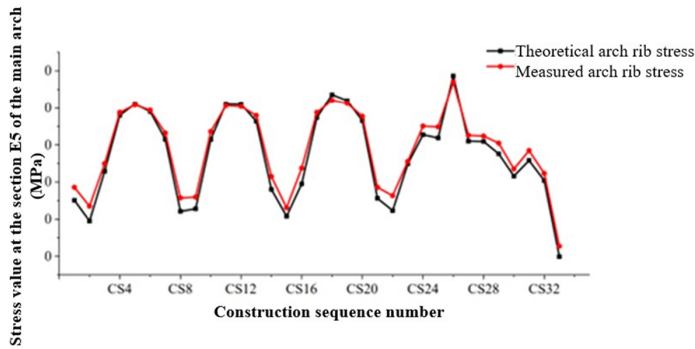


Fig. 22. Comparison values of stress on arch ribs on section E5

6.2. The setting of the pre-camber for the main beam

1. The setting of the pre-camber for the main beam

Based on the actual engineering of this article, the pre-camber is set according to the deflection caused by the dead load plus half of the static live load. The pre-camber at the mid-span is set to be 92.9 mm. The longitudinal section diagram of the construction elevation points of the segmental assembly beam is shown in Fig. 23, and the pre-camber values for the main beam are shown in Table 9.

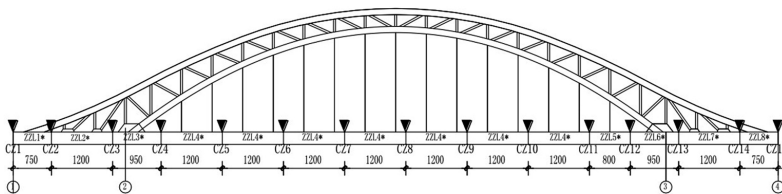


Fig. 23. Longitudinal section diagram of the construction elevation of a segmental assembled beam

Table 9. Designed value of main beam initial camber

Beam segment / Section point	Deflection under dead load (mm)	live load deflection (mm)	pre-camber value of the primary beam (mm)	Beam segment / Section point	Deflection under dead load (mm)	live load deflection (mm)	pre-camber value of the primary beam (mm)
CZ1	0	0	0	CZ9	-73.4	-18.2	82.5
CZ2	-0.3	-1.4	1	CZ10	-51.2	-13.8	59.1
CZ3	0.8	-0.4	-0.6	CZ11	-24.9	-8.2	29
CZ4	-8.8	-3.3	10.5	CZ12	-8.8	-3.4	10.5
CZ5	-33.9	-10.8	39.3	CZ13	0.8	-0.4	-0.6
CZ6	-60.1	-15.8	68	CZ14	-0.3	-1.4	1
CZ7	-78.3	-18.5	87.6	CZ15	0	0	0
CZ8	-82.8	-20.2	92.9				

2. The setting of the pre-camber for the arch ribs

The longitudinal section diagram of the construction elevations for the arch rib nodes is shown in Fig. 24. The pre-camber values for the arch ribs can be found in Table 10.

Table 10. Pre-camber design value of the arch rib

Node	Deflection under dead load (mm)	Live load deflection (mm)	Pre-camber value of the upper arch rib (mm)	Node	Deflection under dead load (mm)	live load deflection (mm)	Pre-camber value of the upper arch rib (mm)
A1	-0.1	-1.5	0.9	A13	-51.2	-10.7	56.6
A2	0.7	-1.1	-0.1	A14	-46	-10.3	51.1
A3	-0.6	-0.3	0.7	A15	-38.7	-9.6	43.5
A4	-3.3	-1.7	4.2	A16	-30.5	-8.6	34.8
A5	-8.2	-3.6	10	A17	-22.2	-7.2	25.8
A6	-14.7	-5.5	17.4	A18	-14.7	-5.5	17.4
A7	-22.2	-7.1	25.8	A19	-8.2	-3.6	10
A8	-30.5	-8.5	34.8	A20	-3.3	-1.7	4.2
A9	-38.7	-9.6	43.5	A21	-0.6	-0.3	0.7
A10	-46	-10.3	51.1	A22	0.7	-1.1	-0.1
A11	-51.2	-10.7	56.6	A23	-0.1	-1.5	0.9
A12	-53.5	-10.9	58.9				

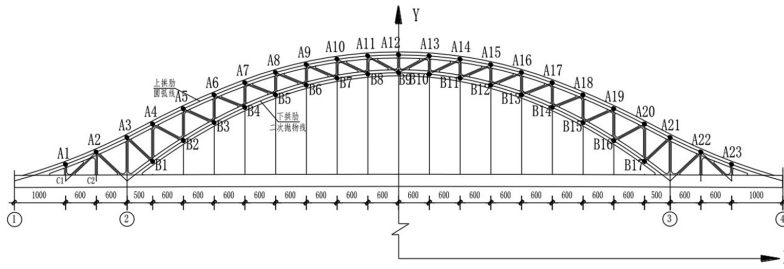


Fig. 24. Longitudinal section diagram of the construction elevation of the arch rib nodes

According to Table 10, it can be seen that the maximum pre-camber value for the main beam occurs at the mid-span position, with a maximum value of 92.9 mm. The maximum pre-camber value for the upper arch rib occurs at node A12, with a maximum value of 58.9 mm. The maximum pre-camber value for the lower arch rib occurs at node B9, with a maximum value of 59.3 mm.

6.3. Monitoring of the line shape during the jacking process

Line shape monitoring of the main beam is carried out during two construction stages: the final stage of jacking and the temporary pier dismantling stage. The specific layout of monitoring points can be found in Fig. 25 and Fig. 26.

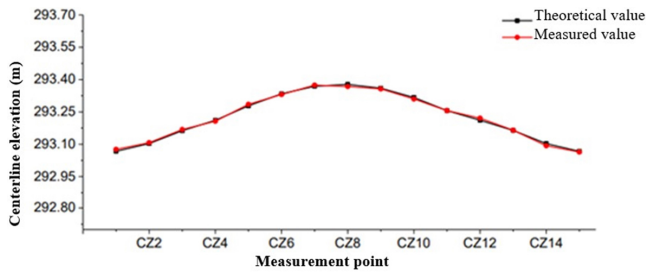


Fig. 25. The alignment of the centerline of the main beam after the completion of top pushing

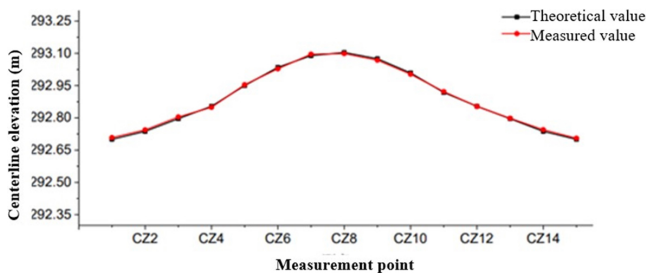


Fig. 26. The alignment of the centerline of the main beam after the removal of temporary piers

Based on the available data, it can be concluded that the theoretical and measured elevations of the monitoring points are generally in good agreement, with no significant errors observed. The difference between the theoretical value and the measured value is within 8 mm, and the difference is within 1%. The deviations of most monitoring points during each construction stage are less than 5mm, and the maximum deviation does not exceed the allowable limit of 8 mm, which remains within the controllable range. This indicates that the construction processes used during the overall jacking and temporary pier dismantling stages are reasonably designed. The on-site monitoring, carried out in accordance with relevant regulations, has achieved a high level of accuracy.

6.4. Results of the suspension rod tension monitoring

After the completion of jacking, the dismantling of the arch ring assembly support and temporary piers is carried out, followed by the tensioning of suspension rods. This process allows for the redistribution of forces throughout the bridge structure, marking a crucial construction stage in the transformation of the structural load system. The detailed values of tensioned forces can be found in Fig. 27 and Fig. 28.

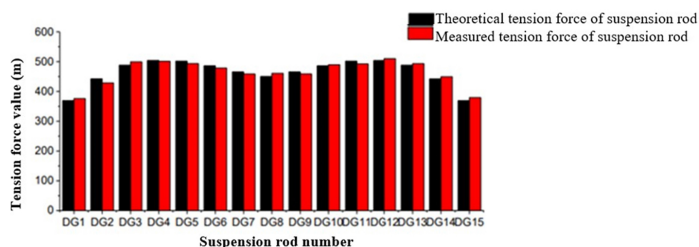


Fig. 27. Upstream cable force ratio

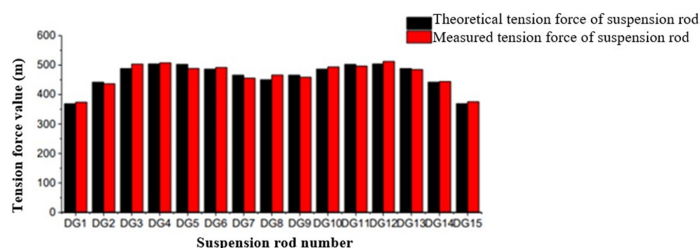


Fig. 28. Downstream cable force ratio

Based on the comparison and analysis of the on-site monitoring data and theoretical data shown in Fig. 27 and Fig. 28, it can be observed that the measured tension forces of the suspension rods during the dismantling of temporary piers stage are very close to the design forces, with differences within $\pm 5\%$. This meets the requirements specified in the regulations. It can be concluded that the overall jacking process in this case is reasonable.

7. Conclusions

1. Based on the analysis of real-time monitoring data during the jacking process of the bridge, the measured stress values of the main girder are within the range of -40.79 MPa to 25.13 MPa, and the measured stress values of the main arch are within the range of -40.33 MPa to 16.06 MPa. These values do not exceed the allowable stress range of the steel during the jacking process, ensuring the structural safety.
2. The measured elevations align well with the theoretical elevations, with deviations mostly less than 5 mm, and the maximum deviation not exceeding the limit of 8 mm.
3. The maximum pre-camber value for the main beam occurs at the mid-span position, with a maximum value of 92.9 mm. The maximum pre-camber value for the upper arch rib occurs, with a maximum value of 58.9 mm. The maximum pre-camber value for the lower arch rib occurs is 59.3 mm.
4. During the dismantling of temporary piers, the measured cable forces of the tensioning cables are very close to the design cable forces, with differences within $\pm 5\%$, which meets the requirements of the specifications. The stress and linear changes during the entire jacking process are stable, indicating that the use of the multi-point continuous jacking method, also known as the incremental launching method, has minimal impact on the structure. This demonstrates that the jacking process ensures structural stability.

References

- [1] C. Jin, "Optimum design of steel truss arch bridges using a hybrid genetic algorithm", *Journal of Constructional Steel Research*, vol. 66, no. 8-9, pp. 1011–1017, 2010, doi: [10.1016/j.jcsr.2010.03.007](https://doi.org/10.1016/j.jcsr.2010.03.007).
- [2] J.W. Wang, H.S. Gao, K.X. Zhang, Z.Y. Mo, and H. Wang, "Seismic performance of horizontal swivel system of asymmetric continuous girder bridge", *Archives of Civil Engineering*, vol. 69, no. 1, pp. 287–306, 2023, doi: [10.24425/ace.2023.144174](https://doi.org/10.24425/ace.2023.144174).
- [3] C. Jin and H. Jin, "Reliability-based optimization of steel truss arch bridges", *International Journal of Steel Structures*, vol. 17, pp. 1415–1425, 2017, doi: [10.1007/s13296-017-1212-y](https://doi.org/10.1007/s13296-017-1212-y).
- [4] H. Gao, H. Duan, Y. Sun, J. Jian, J. Zhang, and H. Liu, "Evaluation of bearing capacity of multi-spanspandrel-braced stone arch bridge based on static load test", *Archives of Civil Engineering*, vol. 68, no. 4, pp. 632–651, 2022, doi: [10.24425/ace.2022.143059](https://doi.org/10.24425/ace.2022.143059).
- [5] H. Gao, K. Zhang, X. Wu, H. Liu, and L. Zhang, "Application of BRB to Seismic Mitigation of Steel Truss Arch Bridge Subjected to Near-Fault Ground Motions", *Buildings*, vol. 12, no. 12, art. no. 2147, 2020, doi: [10.3390/buildings12122147](https://doi.org/10.3390/buildings12122147).
- [6] F. Ma, et al., "Safety Monitoring of Bearing Replacement for a Concrete High-Speed Railway Bridge Based on Acoustic Emission", *Journal of Performance of Constructed Facilities*, vol. 36, no. 3, art. no. 04022014, 2022, doi: [10.1061/\(ASCE\)CF.1943-5509.0001719](https://doi.org/10.1061/(ASCE)CF.1943-5509.0001719).
- [7] P. Zhang, et al., "Key techniques for the largest curved pipe jacking roof to date: A case study of Gongbei tunnel", *Tunnelling and Underground Space Technology*, vol. 59, pp. 134–145, 2016, doi: [10.1016/j.tust.2016.07.001](https://doi.org/10.1016/j.tust.2016.07.001).
- [8] W. Lu and W. Li, "Field monitoring of a tunnel bridge during jacking construction", in *8th International Conference on Reliability, Maintainability and Safety*. IEEE, 2009, pp. 502–506, doi: [10.1109/ICRMS.2009.5270140](https://doi.org/10.1109/ICRMS.2009.5270140).
- [9] P. Lu, H. Shao, and R. Zhao, "Investigation and verification of the fatigue characteristic of the composite bridge deck of a steel truss arch bridge", *Arabian Journal for Science and Engineering*, vol. 42, pp. 1283–1293, 2017.
- [10] R. Li, et al., "Seismic analysis of half-through steel truss arch bridge considering superstructure", *Structural Engineering and Mechanics*, vol. 59, no. 3, pp. 387–401, 2016, doi: [10.12989/sem.2016.59.3.387](https://doi.org/10.12989/sem.2016.59.3.387).

- [11] Q. Chen, et al., "Structural form and experimental research of truss arch bridge with multi-point elastic constraints", *Advances in Structural Engineering*, vol. 24, no.14, pp. 3184–3201, 2021, doi: [10.1177/13694332211020384](https://doi.org/10.1177/13694332211020384).
- [12] L.G. Xu, Y.L. Wang, and C.J. Xu, "Jacking technology for a simply supported girder bridge", *Applied mechanics and materials*, vol. 477, pp. 675–680, 2014, doi: [10.4028/www.scientific.net/AMM.477-478.675](https://doi.org/10.4028/www.scientific.net/AMM.477-478.675).
- [13] Z. Chen, Q.S. Yan, B.Y. Jia, and X.L. Yu, "Large Span Continuous Girder Bridge Jacking Steel Hoop Stress Analysis", *Advanced Materials Research*, vol. 671, pp. 991–995, 2013, doi: [10.4028/www.scientific.net/AMR.671-674.991](https://doi.org/10.4028/www.scientific.net/AMR.671-674.991).
- [14] J. He and X. Gao, "Research of Synchronous Jacking up Construction Monitoring and Control Technologies of Bridge", in *2nd International Conference on Architectural, Civil and Hydraulics Engineering (ICACHE 2016)*. Atlantis Press, 2016, doi: [10.2991/icache-16.2016.7](https://doi.org/10.2991/icache-16.2016.7).
- [15] B. Wan, "Using fiber-reinforced polymer (FRP) composites in bridge construction and monitoring their performance: an overview", in *Advanced composites in bridge construction and repair*. Elsevier, 2014, pp. 3–29, doi: [10.1533/9780857097019.1.3](https://doi.org/10.1533/9780857097019.1.3).
- [16] M. Rashidi, et al., "A decade of modern bridge monitoring using terrestrial laser scanning: Review and future directions", *Remote Sensing*, vol. 12, no. 22, art. no. 3796, 2020, doi: [10.3390/rs12223796](https://doi.org/10.3390/rs12223796).
- [17] H. Fadhil, S.H. Supangkat, and K. Hanafi, "Digital Twin of Road and Bridge Construction Monitoring and Maintenance", in *2022 IEEE International Smart Cities Conference (ISC2)*. IEEE, 2022, doi: [10.1109/ISC255366.2022.9922473](https://doi.org/10.1109/ISC255366.2022.9922473).
- [18] Z. Pan, K. Du, F. Lv, and S. Tao, "Numerical simulation of mechanical response of bridge foundation and existing tunnel caused by pipe jacking construction", *Journal of Physics: Conference Series. IOP Publishing*, vol. 2230, no. 1, art. no. 012008, 2022, doi: [10.1088/1742-6596/2230/1/012008](https://doi.org/10.1088/1742-6596/2230/1/012008).

Received: 2023-10-17, Revised: 2023-12-28